THE JOURNAL OF PHYSICAL CHEMISTRY C

Article

pubs.acs.org/JPCC

Improving the Electrochemical Performance of Si Nanoparticle Anode Material by Synergistic Strategies of Polydopamine and Graphene Oxide Coatings

Chengcheng Fang,[†] Yuanfu Deng,*[,‡] Ye Xie,[‡] Jiangyang Su,[§] and Guohua Chen*[,†,§,∥]

[†]Fok Ying Tung Graduate School, Hong Kong University of Science and Technology, Clear Water Bay, Kowloon, Hong Kong, China

[‡]The Key Laboratory of Fuel Cell for Guangdong Province, School of Chemistry and Chemical Engineering, South China University of Technology, Guangzhou, China

[§]Department of Chemical and Biomolecular Engineering, Hong Kong University of Science and Technology, Clear Water Bay, Kowloon, Hong Kong, China

[∥]Center for Green Products and Processing Technologies, Guangzhou HKUST Fok Ying Tung Research Institute, Guangzhou 511458, China

ABSTRACT: Graphene oxide/polydopamine-coated Si nanocomposite (GO/PDA-Si) was synthesized by a novel facile solution-based chemical method at room temperature. The nanocomposite with a PDA coating layer of ∼1.5 nm exhibits a high reversible specific capacity and excellent cycling stability (1074 mAh g^{-1} after 300 cycles at 2100 mA g^{-1}) as an anode material for lithium ion batteries. The synergistic effect of the PDA coating layer and GO plays an important role in improving the electrochemical lithium storage performances. Both of them can serve as a cushion to buffer the volume change of Si nanoparticles (NPs) during the charge/discharge process and prevent Si NPs from direct contact with a liquid electrolyte. The surface property of Si NPs was also modified by introducing secondary amine groups, which can form amide groups with carboxyl groups and hydrogen bonds with hydroxyl/carboxyl groups on GO. These chemical interactions firmly anchor Si NPs to GO so that aggregation of Si NPs can be mostly prevented. Moreover, the good lithium ion conductivity of PDA is beneficial for rate performance. The experimental results should be very useful in guiding the preparation of long-cycle-life Si-based anode materials with good rate performance using a simple surface-modification process.

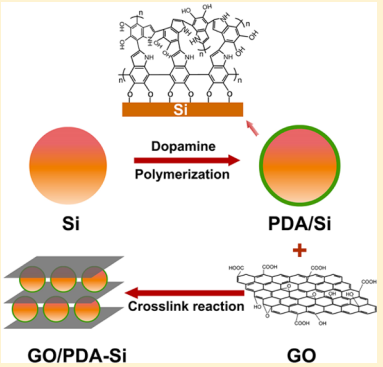

INTRODUCTION

With the rapid developments of portable electronic devices, electric vehicles (EVs), hybrid electric vehicles (HEVs), and large-scale energy storage, it urgently requests a significant improvement in electrochemical performances, including specific capacity, cycling stability, and rate capability, of the electrode materials for lithium ion batteries (LIBs) to meet the increasing energy and power density demands of LIBs.[1,2] Among the various types of anode materials, silicon (Si) is considered as one of the most promising candidates for next-generation high-performance LIBs, due to its extremely high theoretical specific capacity (up to 4200 mAh g^{-1}), low operating potential (<0.5 V vs Li/Li^+), natural abundance and environmental benignity.[3−5] However, the electronic conductivity of Si is poor. Moreover, the large volume change of Si, which is more than 300%, during alloying/dealloying process causes severe internal stress, resulting in capacity fading because of dramatic electrode pulverization and lose of electrical contact with current collector.[6] Meanwhile, the large volume change would damage the solid electrolyte interface (SEI) layer, which is formed on the surface of Si active material in the initial several cycles. This may lead to continuous formation of SEI layers to eventually deplete the electrolyte.[7]

To overcome the above-mentioned problems, a variety of nanostructured Si have been synthesized, such as Si nanowires,[8,9] nanotubes,[10] and nanospheres.[11] Since nanosized Si-based materials could shorten the diffusion lengths of electrons and lithium ions. The small sized particles are more resistant to internal stress caused by volume variations.[12,13] Nanosized Si, however, have the tendency of aggregation. It requires proper immobilization to make a good Si anode. The formation of Si/C nanocomposite is believed to be another good way to improve the poor electrical conductivity of Si, alleviate severe volume expansions, and prevent the agglomeration of Si nanomaterials in the electrode.[14,15] Especially, for carbon-coated Si nanocomposite, the carbon coating layer could avoid the direct exposure of Si to electrolyte, which helps the stabilization of SEI films.[7] In recent years, graphene nanosheets, two-dimensional monolayers of graphitic carbon, have been widely utilized with Si nanomaterials to form graphene-encapsulated Si nanocomposites, due to the excellent conductivity, large surface area, high mechanical flexibility,

Received: November 7, 2014
Revised: December 25, 2014
Published: January 9, 2015

DOI: 10.1021/jp511179s
J. Phys. Chem. C 2015, 119, 1720−1728

and chemical stability of graphene, which are very helpful in improving the electrochemical performances of Si-based anode.[16−18]

One commonly used method of fabricating Si/graphene nanocomposites is to physically blend preobtained Si nanocrystals and graphene sheets or GO by methods such as suction filtration,[19] freeze-drying[20] or ball milling.[21] Once GO is used, a thermal treatment or a hydrazine reduction is conducted subsequently to reduce the GO into graphene.[22] In spite of the facilitation of the physical blending methods, there are several obstacles to overcome to obtain uniform Si/graphene nanocomposites. First, Si nanocrystals are prone to agglomeration in aqueous solution due to the large surface areas. Second, the interaction between Si and graphene is not sufficiently strong to keep the contact intact when Si nanocrystals experience continuous volume variations during the charge/discharge processes.[23,24] Therefore, it is highly desirable to anchor Si nanocrystals onto graphene sheets via chemical bonds or electrostatic attraction to enhance the structural stability.[25,26] In this regard, Yang and co-workers reported covalently bonded Si NPs to the surface of aminophenyl modified graphene sheets via aromatic linkers through diazonium chemistry.[27] Wang's group synthesized graphene bonded and encapsulated aminopropyltrimethoxysilane (APS)-functionalized Si NPs by aerosol spray method.[28] The trimethoxysilane group of APS would react with the SiO_2 layer on the surface of Si NPs and the amino group on the other end of APS would interact with the carboxyl groups on GO, forming strong chemical bonds between Si and GO. Our group also successfully constructed interfacial bonding between Si NPs and GO by a two-step chemical strategy using aminopropyltriethoxysilane (APTES) as the intermediate.[29] Li and co-workers developed polyaniline-functionalized Si NPs and subsequently wrapped them with GO via a $\pi-\pi$ interaction and electrostatic attraction between the GO and polyaniline.[30] The Si/graphene nanocomposites so prepared have shown much improved electrochemical performances. The complicated chemical procedures and the highly dangerous chemical reactions (e.g., HF pretreatment of Si NPs and diazonium reaction) involved, however, make them difficult to scale up.

Dopamine, which can self-polymerize and spontaneously deposit conformal polydopamine (PDA) films on almost any surfaces under basic conditions,[31] has been utilized as a precursor to form carbon-coated metal oxides[32,33] and silicon[7] as anode materials for LIBs. PDA functionalized Si NPs can interact with GO sheets to stabilize Si NPs on GO and lead to enhanced electrochemical performance, because (1) the secondary amine groups on PDA layer could form amide groups with carboxyl groups and hydrogen bonds with hydroxyl groups on GO, (2) these chemical interactions firmly anchor Si NPs to GO so that aggregations of Si NPs could be prevented effectively, (3) the surface-coated PDA, a soft and elastic polymer layer, can serve as a buffer to alleviate the large volume expansions of Si NPs and avoid the direct contacts between Si NPs and liquid electrolyte, which are beneficial for stable SEI layers and high Coulombic efficiency, and (4) the PDA exhibits a good conductivity for lithium ions.[31] The merit of such a Si-GO composite lies in that the chemical process is very facile and easy to scale up. Hence, it becomes the objective of the present study. As expected, a much improved cycling performance and rate capability of the as-prepared GO/PDA-Si nanocomposite was obtained. A discharge capacity of 1074 mAh g^{-1} was maintained after 300 cycles at 2100 mA g^{-1}. Detailed analysis on the fabrication and characterization of the GO/PDA-Si nanocomposite is given subsequently.

EXPERIMENTAL SECTION

Preparation of GO. The GO was synthesized by the famous modified Hummer's method.[34] In a typical experiment, 46 mL of concentrated sulfuric acid was added into a 500 mL three-necked flask immersed in ice bath. In total, 2.0 g of graphite flake and 1.0 g of sodium nitrate were added into the continuously stirred sulfuric acid. Then 6.0 g of potassium permanganate was added into the mixture slowly, keeping the temperature below 10 °C and stirring for 1 h. The temperature was then raised to 35 °C and maintained there for 2 h while manitaining on stirring. Subsequently, 92 mL of deionized water was dropwise added into the suspension with continued stirring for another 15 min. A volume of 280 mL of deionized water was added to terminate the reaction. Afterward, 10 mL of 30% H_2O_2 was added to react with the residual potassium permanganate until the color of the suspension changed to bright yellow. Next, 24 mL of 5% HCl was added to wash the residual metallic ions. The obtained oxidized graphite suspension was washed with deionized water by centrifugation for several times until the solution became neutral. The product was finally treated with ultrasonic for 2 h, followed by centrifuging at 10 000 rpm for 15 min. The GO was obtained in the supernatant and diluted in deionized water to a concentration of 1 mg mL^{-1}.

Preparation of GO/PDA-Si. In total, 1.0 g of polyvinylpyrrolidone (PVP) was dissolved into 95 mL of supernatant water and kept stirring for 1 h. In total, 100 mg of Si NPs (~100 nm, Alfa Aesar) was added into the PVP solution and treated ultrasonically for 20 min to homogeneously disperse the nanoparticles in the solution. In total, 0.6 g of tris(hydroxymethyl)aminomethane was added, followed by adjusting the pH to 8.5 by diluted hydrochloric acid. After that, 0.1 g of dopamine hydrochloride was dissolved in 5 mL of distilled water and then added into the above suspension. After sonicating for 30 min, the suspension was kept stirring for 7.5 h at room temperature. PDA-coated Si NPs were then collected by vacuum filtration and mixed with two desired amouns of GO (1 mg mL^{-1}) with stirring for 1 h. Then GO/PDA-Si nanocomposite was collected by centrifuging at 8 000 rpm for 10 min. It was first dried at 80 °C for 8 h and then dried at 150 °C for 2 h under vacuum to form cross-link reaction between secondary amine groups on PDA and carboxyl groups on GO. The samples with 0, 21.5, 43 mL of GO were named GO/PDA-Si_0, GO/PDA-Si_1, and GO/PDA-Si_2, respectively. GO/Si was also prepared by physically mixing Si NPs and 43 mL of GO aqueous solution for comparison.

Physical Characterizations. The morphologies were characterized by scanning electron microscopy (SEM, JEOL JSM 6700F) and transmission electron microscopy (TEM, JEOL 2010F). Fourier transform-infrared spectroscopies (FT-IR) were documented with KBr pellets by Bruker R 200-L spectrophotometer. X-ray photoelectron spectroscopy (XPS) measurements were conducted by a Kratos Axis Ultra spectrometer with focused monochromatic Al Kα radiation ($h\nu$ = 1486.6 eV). Thermogravimetric analyses (TGA) were measured by a thermogravimetric analyzer (TA Instruments, model TGAQ50).

Electrode Fabrication and Electrochemical Tests. The tests were measured in CR2025 coin half-cells. The working electrode was fabricated by pasting slurry, containing Si

DOI: 10.1021/jp511179s
J. Phys. Chem. C 2015, 119, 1720−1728

nanocomposite, carbon black, and sodium alginate in a mass ratio of 60:20:20 in water, onto copper foil with a mass loading of ~1.5 mg, and dried at 80 °C for 12 h under vacuum. The selection of sodium alginate as a binder here is because the carboxyl groups and hydroxyl groups of sodium alginate have chemical interactions with GO and PDA, which can make the whole structure of the electrode more stable.[29] The dried electrodes were pressed at 10 MPa. The electrolyte was 1.0 M $LiPF_6$ in ethylene carbonate (EC), ethyl methyl carbonate (EMC), and dimethyl carbonate (DMC) (1:1:1, v/v/v) with 3 wt % of vinylene carbonate (VC). Celgard 2400 was used as the separator. Cells were assembled in an Ar-filled glovebox (Master 100 Lab, Braun, Germany) with less than 1 ppm of oxygen and moisture. The galvanostatic charge/discharge performances were tested on a multichannel battery test system (Neware, CT-3008W) between 0.01 and 1.0 V at different rates. The cyclic voltammetric (CV) tests were performed on an electrochemical workstation (Autolab PGSTAT 101) at a scan rate of 0.1 mV s^{-1}. The electrochemical impedance spectroscopy (EIS) analysis was carried out at room temperature with a Versa-stat 3 electrochemical workstation (Princeton Applied Research) with a frequency range from 100 kHz to 10 mHz.

RESULTS AND DISCUSSION

The synthetic procedures of GO/PDA-Si nanocomposite are schematically illustrated in Scheme 1. The Si NPs were coated by PDA in dopamine hydrochloride aqueous solution with a concentration of 1.0 g L^{-1} and pH of 8.5. In terms of the coating mechanism, it has been reported that the catechol-derivative anchor groups on dopamine show a strong and irreversible binding affinity to the surface hydroxyl groups of metal oxides (e.g., Fe_3O_4[32]) in aqueous solution, resulting in dehydration reaction and formation of a charge transfer complex. Then, a conformal and continuous PDA layer could form on the solid surface through oxidation, cyclization, and polymerization reactions. For Si NPs, it contains a layer of amorphous oxidized SiO_2, which also could form numerous surface Si−OH bonds in aqueous solution,[35] sharing the similar coating mechanism with metal oxides. The PDA-coated Si NPs were subsequently mixed with GO solution. In order to obtain a cross-link reaction between secondary amine groups on PDA and carboxyl groups on GO, the collected GO/PDA-Si nanocomposite was further dried at 150 °C for 2 h under vacuum.

Scheme 1. Schematic Illustration of the Synthetic Procedures of GO/PDA-Si Nanocomposite

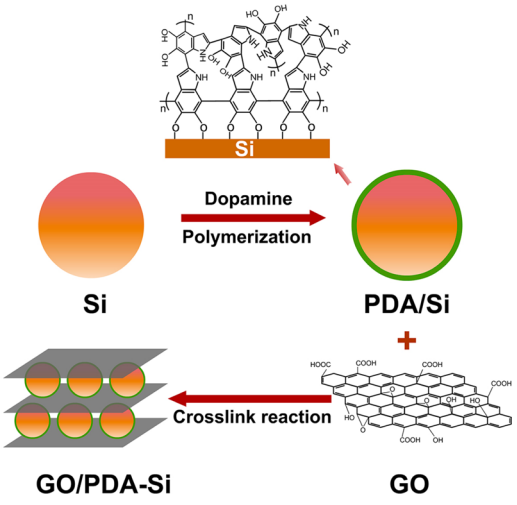

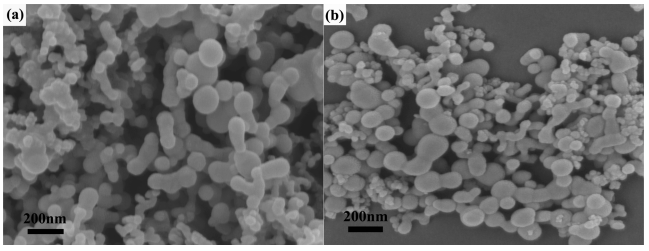

Figure 1. SEM images of (a) pristine Si NPs and (b) GO/PDA-Si_0.

Comparing the SEM image of GO/PDA-Si_0 (Figure 1b) with that of pristine Si NPs (Figure 1a), no significant differences can be observed, except for the surface of pristine Si NPs is smoother. The relatively rough surface of GO/PDA-Si_0 may be caused by the PDA-coating layer. For both samples, the particle size ranges from 50 to 150 nm with some fines dispersed around.

Figure 2 shows the SEM images of GO/PDA-Si_1 (Figure 2a), GO/PDA-Si_2 (Figure 2b), and GO/Si mixture (Figure 2c). It is clear to see that Si NPs are well dispersed in sample GO/PDA-Si_1 and GO/PDA-Si_2. The SEM images of the two samples show no significant differences. For GO/Si composite without PDA coating, it shows that most of the unmodified Si NPs agglomerate together and only a small portion of them is wrapped by GO sheets. The results demonstrate that PDA coating can effectively prevent the agglomeration of Si NPs and lead to a homogeneous dispersion of Si NPs on GO. First, the coating layer avoids direct contacts among Si NPs. Second, the covalent and hydrogen bonding interactions between PDA and GO sheets could firmly immobilize the Si NPs on GO sheets.

Figure 3 displays the TEM and HRTEM images of the GO/PDA-Si_0 (Figure 3a,c) and GO/PDA-Si_2 (Figure 3b,d). As pointed out in Figure 3a, the irregular part is the fine particles of Si, which can also be observed in SEM images. The TEM image in Figure 3b exhibits that the diameters of PDA-coated Si NPs range from 50 to 100 nm and they are wrapped by GO sheets, in accordance with the SEM observation (Figure 2b). Figure 3c shows the HRTEM image of PDA-coated Si NP and the purchased pure Si NP (inset in Figure 3c). The original oxidized layer of SiO_2 on the Si NP is about 1 nm. After PDA coating, the thickness of the amorphous layer increased to ~2.5 nm, suggesting the PDA layer is about ~1.5 nm. The HRTEM image of an edge part of GO/PDA-Si_2 nanocomposite shown in Figure 3d further confirms that PDA-coated Si NPs are well encapsulated in the GO matrix, as it is clear to see the fringe of GO in the outermost layer.

FT-IR spectra were obtained to confirm successful coating of PDA on the Si NPs (Figure 4a) and the formation of chemical bonds between PDA and GO (Figure 4b). In the spectrum of Si NPs, the peak at 3775 cm^{-1} is attributed to the stretching of free silanol group.[36] For the GO/PDA-Si_0, the peak at 3775 cm^{-1} becomes much weaker, and meanwhile, two more peaks at 2926 and 2857 cm^{-1}, attributing to the vibrations of methyl/methylene in PDA,[23] can be observed. These evidence indicate PDA has been successfully coated onto Si NPs. For comparison, the FT-IR spectra of the GO/Si and GO/PDA-Si_2 are also displayed. As shown in in Figure 4b, the region

DOI: 10.1021/jp511179s
J. Phys. Chem. C 2015, 119, 1720−1728

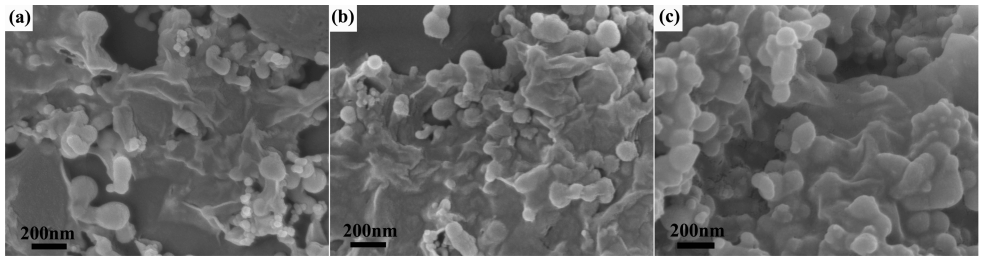

Figure 2. SEM images of (a) GO/PDA-Si_1, (b) GO/PDA-Si_2, and (c) GO/Si.

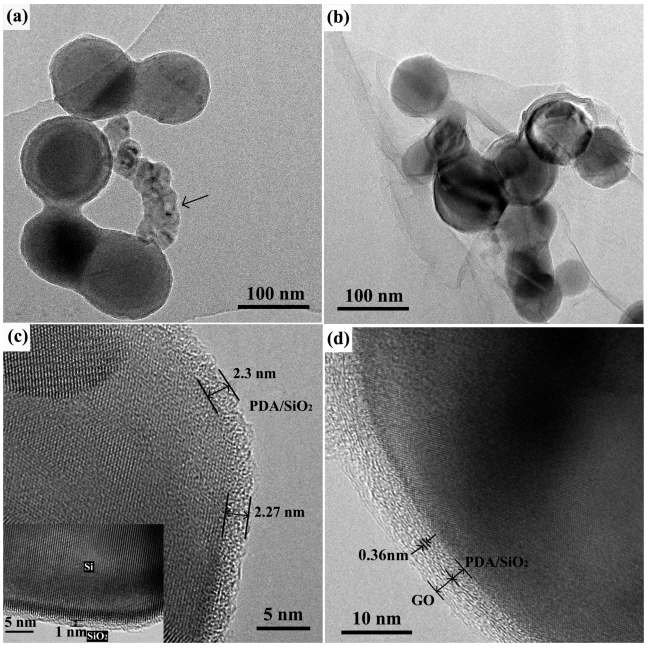

Figure 3. TEM images of (a) GO/PDA-Si_0 and (b) GO/PDA-Si_2; HRTEM images of (c) GO/PDA-Si_0 and (d) GO/PDA-Si_2.

from 3630 to 3010 cm^{-1} represents the hydrogen bond domain and the strong peak around 3430 cm^{-1} is ascribed to −OH stretching vibration.[37] Because of the increasing degree of intermolecular association, the −OH peaks become broader and shift to lower frequency (the sharp band for free −OH usually locate at 3650−3610 cm^{-1}), suggesting the intermolecular hydrogen bonding interactions (N−H/O−H, N−H/N−H or O−H/O−H) in the two samples.[38] For GO/Si sample, the presence of the strong peak at 3757 cm^{-1} illustrates that no obvious interactions between Si NPs and GO. The peak at 1632 cm^{-1} is attributed to aromatic C═C stretching vibration. The peaks at 1736 and 1394 cm^{-1} correspond to the stretching vibration of C═O and bending vibration of O−H for carboxyl groups on GO. The absorption at 1043 cm^{-1} is due to the stretching vibration of C−O for C−OH on GO.[38] For GO/PDA-Si_2 nanocomposite, the relative intensities of peaks at 1736 and 1394 cm^{-1} decreased obviously and the peak at 1552 cm^{-1} disappeared. According to a previously published result, the peak at 1632 cm^{-1} may be due to the C═O stretching vibration of amide.[39] These results suggest the cross-link reactions between the secondary amine groups on PDA and the carboxyl groups on GO. The peak of GO/PDA-Si_2 at 1043 cm^{-1} decreased and became broader, which might be due to some hydrogen bonding interactions between the secondary amine groups on PDA and hydroxyl groups on GO.[29]

XPS measurements were conducted to characterize the elemental composition and further confirm the chemical interactions between PDA and GO. Figure 5a shows the full XPS spectra of the as-prepared GO/PDA-Si_0 and GO/PDA-Si_2 samples. For GO/PDA-Si_0, the presence of C and N suggests the successful coating of PDA layer. In the spectrum of GO/PDA-Si_2, the intensity of Si 2p, Si 2s, and N 1s obviously decreased while the intensity of C 1s increased comparing with GO/PDA-Si_0 sample, indicating that PDA-coated Si NPs have been encapsulated by GO sheets. As shown in Figure 5b, the C═C at 284.2 eV, C−C at 285.3 eV and C−O/C−N at 287.1 eV can be observed for C 1s of GO/PDA-Si_0. The presence of PDA can be confirmed by the N 1s spectrum (Figure 5c). The peaks at 399.2 and 400.1 eV are assigned to free -NH and hydrogen-bonded -NH, respectively. As to GO/PDA-Si_2, the C 1s core level peak of the nanocomposite can split into four components centered at 284.4, 285.0, 286.8, and 288.2 eV, corresponding to the aromatic C═C bonds, C−C bonds, C−O/C−N bonds, and O−C═O bonds, respectively (Figure 5d). For N 1s spectrum, as shown in Figure 5e, two peaks at 400.1 and 402.2 eV can be observed, which can be

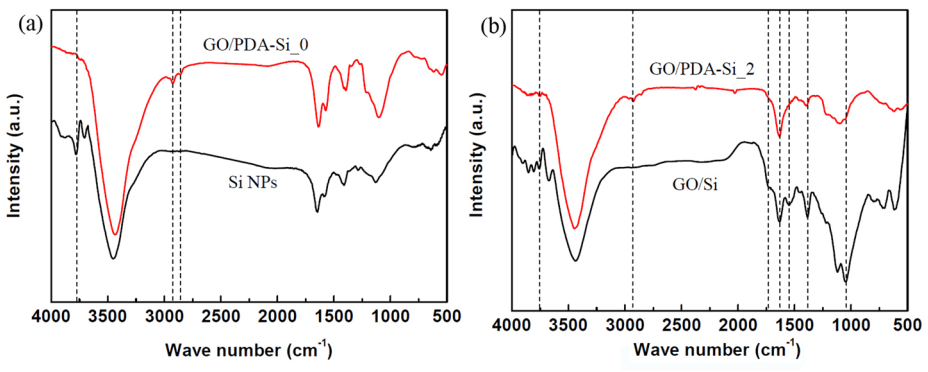

Figure 4. Fourier transform infrared (FT-IR) spectra of (a) pristine Si NPs and GO/PDA-Si_0 and (b) GO/Si and GO/PDA-Si_2.

DOI: 10.1021/jp511179s
J. Phys. Chem. C 2015, 119, 1720−1728

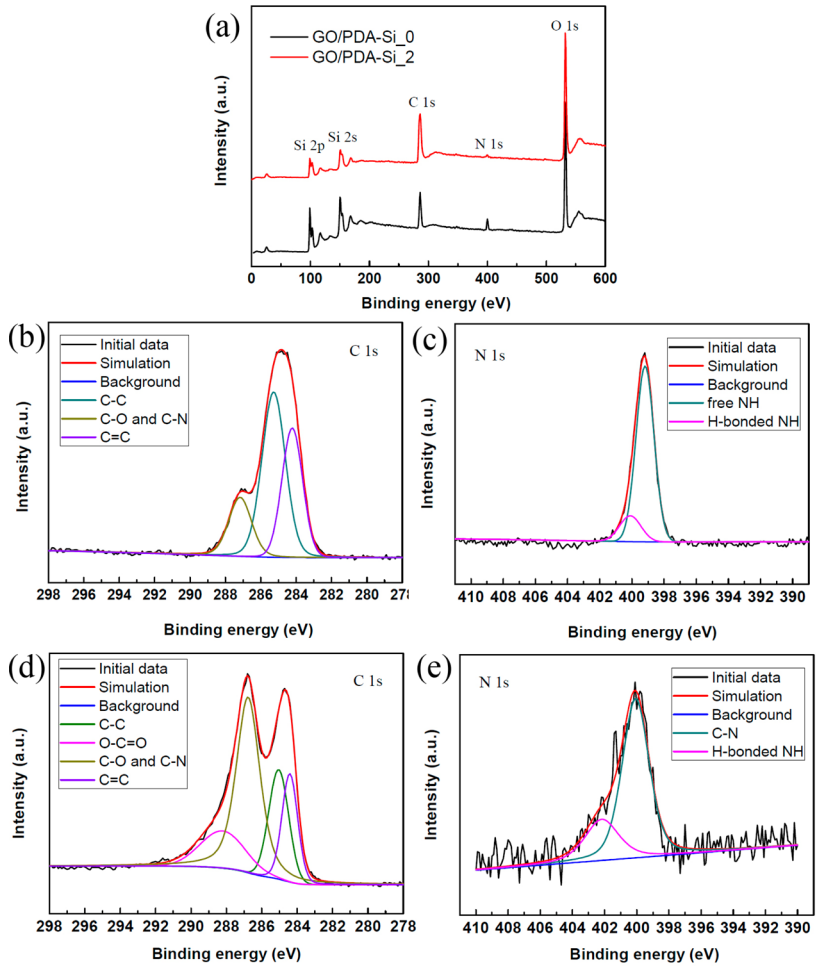

Figure 5. (a) XPS spectra of GO/PDA-Si_0 and GO/PDA-Si_2; (b) C 1s spectrum of GO/PDA-Si_0; (c) N 1s spectrum of GO/PDA-Si_0; (d) C 1s spectrum of GO/PDA-Si_2; and (e) N 1s spectrum of GO/PDA-Si_2.

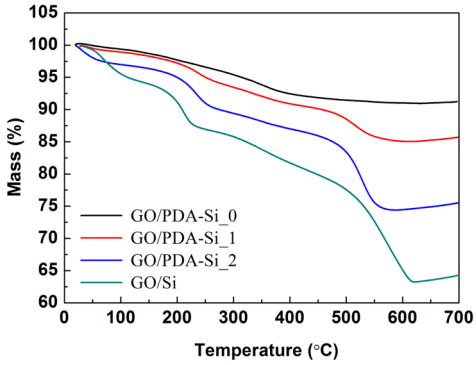

Figure 6. TGA curves of GO/Si, GO/PDA-Si_0, GO/PDA-Si_1, and GO/PDA-Si_2.

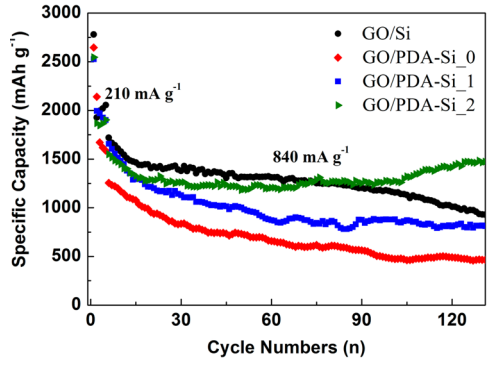

Figure 7. Cyclic performance of GO/Si, GO/PDA-Si_0, GO/PDA-Si_1, and GO/PDA-Si_2.

assigned to N 1s spectrum of amide (C−N) and strong hydrogen-bonded −NH.[29] The XPS results further confirmed the successful coating of PDA on Si NPs and the subsequent formation of covalent bonding and hydrogen bonding interactions between PDA and GO sheets.

Samples with different amount of GO were carried out to illustrate the influence of GO on electrochemical performances of PDA/Si composite. TGA was used to determine the compositions of GO/PDA-Si_0, GO/PDA-Si_1, GO/PDA-Si_2, and GO/Si samples (Figure 6). The mass loss below 150 °C corresponds to the loss of absorbed water molecules on the surfaces of the samples. The mass loss of water for GO/PDA-Si_0, GO/PDA-Si_1, GO/PDA-Si_2, and GO/Si are 1.5%, 2.0%, 3.5%, and 6.0%, respectively. The curve of GO/PDA-Si_0 sample illustrates that the oxidation of PDA occurs between 150 and 550 °C and the mass percentage of PDA in the composite is 7.6% and Si NPs is 92.4%. Since the PDA-Si sample is the intermediate material for the preparations of both GO/PDA-Si_1 and GO/PDA-Si_2, the mass ratios of PDA and Si NPs in these two samples should be the same. For both GO/PDA-Si_1 and GO/PDA-Si_2, the mass loss between 150

DOI: 10.1021/jp511179s
J. Phys. Chem. C 2015, 119, 1720−1728

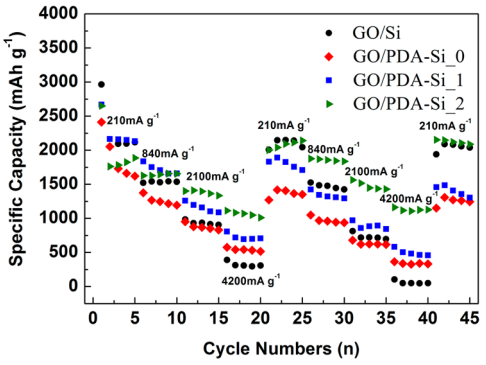

Figure 8. Rate performance of GO/Si, GO/PDA-Si_0, GO/PDA-Si_1, and GO/PDA-Si_2.

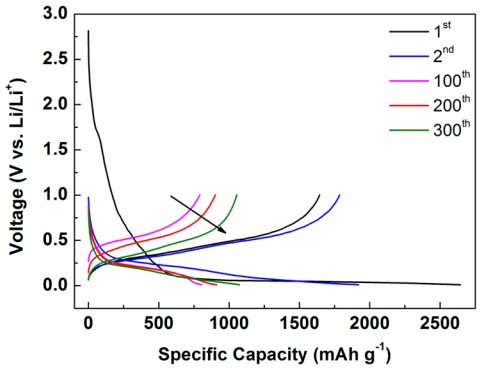

Figure 9. Galvanostatic charge/discharge profiles of GO/PDA-Si_2 at different cycles.

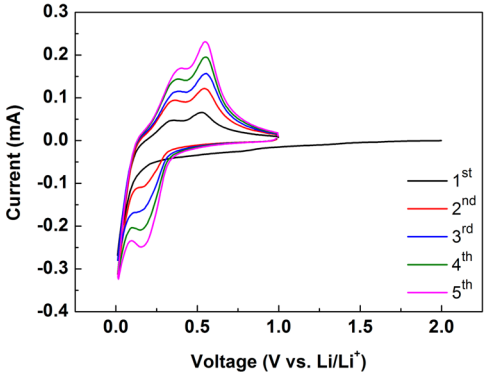

Figure 10. CV curves of the initial five cycles of GO/PDA-Si_2.

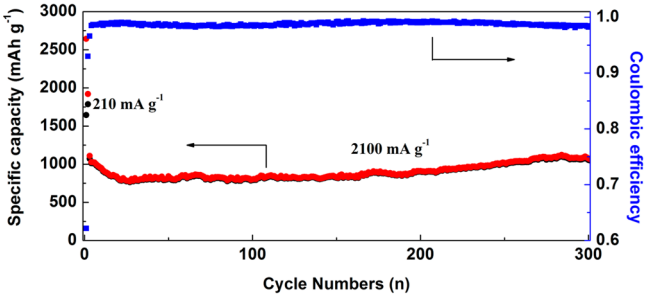

Figure 11. Coulombic efficiency and capacity retention of GO/PDA-Si_2 at 2100 mA g^{-1}.

and 600 °C corresponds to the oxidation of PDA and GO. Above 600 °C, the curves gradually increase, ascribing to the oxidation of Si core. On the basis of the above analysis, the compositions of GO/PDA-Si_1, GO/PDA-Si_2, and GO/Si can be calculated. For GO/PDA-Si_1, the corresponding data are 86.2%, 6.1%, and 7.1%, respectively. For GO/PDA-Si_2, the mass percentages of Si, GO, and PDA are 77.2%, 16.5%, and 6.3%, respectively. For GO/Si, the mass percentages of Si and GO are 67% and 33%, respectively.

On the basis of the aforementioned SEM, (HR)TEM, FT-IR, XPS, and TGA characterization results, it has been verified that a thin PDA layer was successfully coated on the surface of Si NPs and the PDA-coated Si NPs were firmly immobilized on GO sheets via the covalent bonding and hydrogen bonding interactions between PDA and GO. The as-prepared GO/PDA-Si nanocomposites, as anode materials for LIBs, are expected to deliver an enhanced electrochemical lithium storage performance. The coating layer avoids direct contact of Si NPs and electrolyte. The functional groups on PDA anchored Si NPs on GO through chemical bonds, which could prevent the agglomeration of Si NPs during extended cycles. The flexible polymer layer can also buffer the large volume change of Si NPs during the charge/discharge process. Furthermore, the PDA layer could facilitate the diffusion of lithium ions due to its good lithium ion conductivity.

Figure 7 compares the cyclic performances of the GO/PDA-Si_0, GO/PDA-Si_1, and GO/PDA-Si_2 along with the one without PDA coating (GO/Si). The electrodes were first activated for 5 cycles at a current density of 210 mA g^{-1} and then charged/discharged at 840 mA g^{-1} for extended cycles between 0.01 and 1 V. Comparing the cyclic performance of the GO/Si and GO/PDA-Si_2 samples, the influence of PDA coating layer can be illustrated. Although the specific capacity of GO/Si is higher than that of GO/PDA-Si_2 in the first 75 cycles, the GO/PDA-Si_2 sample exhibits a much better cycling stability than that of the GO/Si sample. The high specific capacity of the GO/Si sample in the first several cycles is due to the high content of GO in this sample, which can enhance the electrical conductivity, facilitating charge transfer during the charge/discharge process. After 130 cycles, the discharge capacity of the GO/Si mixture only maintains 925 mAh g^{-1} and an obvious tendency of capacity fading can be observed, which is ascribed to the weak interactions between Si NPs and GO sheets, as demonstrated by the SEM image and FT-IR spectrum. The comparison of the GO/PDA-Si_0, GO/PDA-Si_1, and GO/PDA-Si_2 nanocomposites can illustrate the effects of GO on the electrochemical performances of these samples. The discharge capacity of GO/PDA-Si_0 drops very fast and only remains at 465 mAh g^{-1} after 130 cycles. The poor cycle performance of GO/PDA-Si_0 is attributed to the poor the conductivity of this sample, which can be demonstrated by the largest internal impedance before and after cycles among the four samples (Figure 12). In addition, the PDA coating layer on the surface of Si alone may be not enough to buffer the large volume change of Si nanoparticles, resulting in its poor cycle performance. By adding small amount of GO (6.1 wt %), the specific capacity increases obviously and the cycling stability has also been slightly enhanced (as shown in the GO/PDA-Si_1 sample). Further adding the mass of GO up to 16.5 wt %, the cyclic performance has been improved significantly (as demonstrated by the GO/PDA-Si_2). The GO/PDA-Si_2 sample shows a high specific discharge capacity of 1475 mAh g^{-1} after 130 cycles while GO/PDA-Si_1 only remains 814 mAh g^{-1}. This result demonstrates that the GO/PDA-Si_2 may have formed a more stable SEI layer during the

DOI: 10.1021/jp511179s
J. Phys. Chem. C 2015, 119, 1720−1728

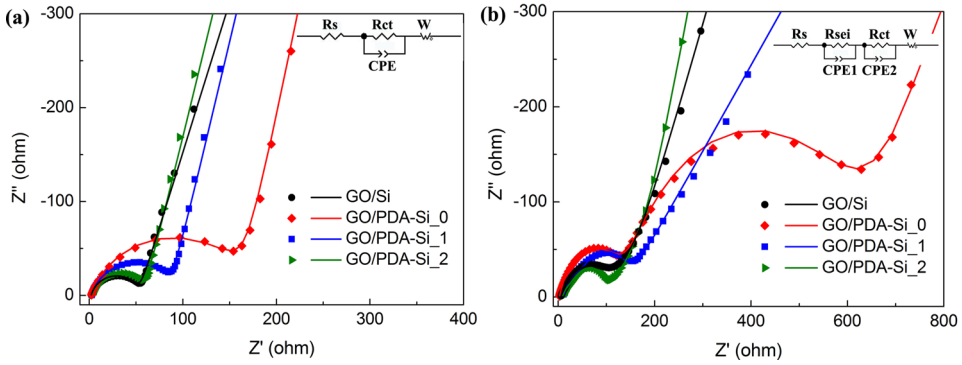

Figure 12. Nyquist plots of GO/Si, GO/PDA-Si_0, GO/PDA-Si_1, and GO/PDA-Si_2 anodes (a) before cycle and (b) after 100 cycles at 840 mA g^{-1}.

Table 1. EIS Fitting Result of GO/Si, GO/PDA-Si_0, GO/PDA-Si_1, and GO/PDA-Si_2 Samples before and after Cycles

samples	cycle number	Rs (ohm)	Rsei (ohm)	Rct (ohm)
GO/Si	before cycle	1.96		50.76
	after 100 cycles	4.30	15.45	69.44
GO/PDA-Si_0	before cycle	2.09		160.91
	after 100 cycles	2.37	131.41	483.40
GO/PDA-Si_1	before cycle	2.46		83.92
	after 100 cycles	10.35	33.49	85.66
GO/PDA-Si_2	before cycle	2.65		56.16
	after 100 cycles	9.12	13.22	66.16

initial 20 cycles due to the sufficient amount of GO, which can wrap the PDA-coated Si NPs up and thus prevent the direct contact of Si NPs and electrolyte. On the basis of the improved cycle performance of GO/PDA-Si_2, it is suggested that the GO and PDA have synergetic effects on the cycle performance of the Si NPs. On one hand, the GO sheets can significantly improve the electrical conductivity of the nanocomposite, avoid the exposure of Si NPs to electrolyte, and act as a buffer to alleviate the volume change of Si NPs. On the other hand, the PDA coating layer tightly anchors Si NPs to GO sheets through the covalent and hydrogen bonding interactions, preventing the aggregation of particles and further buffering the volume expansion during charging/discharging processes.

Figure 8 shows the rate performance of the above-mentioned four samples. As expected, the GO/PDA-Si_2 sample also exhibits the best rate capability among these four. It delivers discharge capacities of 1887, 1657.6, 1409, and 1082 mAh g^{-1} at current densities of 210, 840, 2100, and 4200 mA g^{-1}, respectively. When the current density returns to 210 mA g^{-1}, the capacity goes back to 2003.4 mAh g^{-1}, indicating the superior rate reversibility. It is worthy to mention that, at low current densities of 210 and 840 mA g^{-1}, the specific capacity of the GO/PDA-Si_2 sample is comparable to that of the GO/Si sample. However, the much higher specific capacity of the GO/PDA-Si_2 sample is observed when the discharge/charge current density increases to 4200 mA g^{-1} (the capacities of GO/PDA-Si_0, GO/PDA-Si_1, GO/PDA-Si_2, and GO/Si are 542, 718, 1082, and 314 mAh g^{-1}, respectively). These results demonstrate that the GO and PDA also have synergetic effects on the rate performance of the Si NPs. The chemical cross-linked and hydrogen bonding interactions formed between PDA and GO and the good ionic conductivity of the PDA together lead to the enhanced rate capabilities of the GO/PDA-Si_2 sample.

Figure 9 displays the galvanostatic charge/discharge curves of the GO/PDA-Si_2 sample, in which the first two cycles are activated at 210 mA g^{-1} and the following cycles are tested at 2100 mA g^{-1} between 0.01 to 1.0 V vs Li/Li^+. The initial discharge/charge capacities are 2643 and 1643 mAh g^{-1}, respectively, with Coulombic efficiency being 62.2%. The large irreversible capacity loss in the first cycle can be ascribed to the formation of SEI film and the irreversible lithium consumption of GO. For the 100th, 200th, and 300th cycles, the capacity increased obviously, which can be attributed to the improvement of lithium ion accessibility during extended cycles and thus the voltage hysteresis gradually decreases.

Typical CV curves of GO/PDA-Si_2, with a potential window of open circuit voltage to 0.01 V for the first cycle and 1 to 0.01 V for the following four cycles at scanning rate of 0.1 mV s^{-1}, are shown in Figure 10. In the first cycle, a broad cathodic peak between 0.9 to 0.5 V relates to the formation of SEI layer and disappears in subsequent cycles. The sharp peak below 0.25 V represents the insertion of lithium ions into Si NPs. The two anodic peaks at 0.37 and 0.55 V are assigned to the dealloying of Li−Si alloy. In subsequent cycles, the cathodic peaks at 0.17 correspond to the generation of Li−Si alloy phase.[40] Noticeably, the intensity of both cathodic peaks at 0.17 V and anodic peaks at 0.37 and 0.55 V gradually increases in the initial five cycles, which may be due to the existence of the activating process in the GO/PDA-Si_2-based anode.

Figure 11 shows the cyclic performance of GO/PDA-Si_2. A reversible discharge capacity of 1074 mAh g^{-1} is maintained after 300 cycles at a high current density of 2100 mA g^{-1}, indicating the GO/PDA-Si_2 sample exhibits both excellent cyclic stability and good rate capability.

EIS measurements are carried out to further understand the different electrochemical behaviors of the GO/Si, GO/PDA-Si_0, GO/PDA-Si_1, and GO/PDA-Si_2 samples. Before cycling, GO/Si sample shows the least impedance among the four samples due to the sufficient amount of GO, as displayed in Figure 12a. In Figure 12b, the Nyquist plots of half cells based on the four samples are performed after 100 cycles under the current density of 840 mA g^{-1}. The fitting results are listed in Table 1. The GO/PDA-Si_0 sample shows the largest ohmic resistance among the four samples, due to the absence of GO, leading to poor electrical conductivity and large pulverization. As expected, the impedance of GO/PDA-Si_1 is larger than that of GO/PDA-Si_2. Comparing the GO/Si and GO/PDA-Si_2, GO/PDA-Si_2 shows a less ohmic resistance. This can be

DOI: 10.1021/jp511179s
J. Phys. Chem. C 2015, 119, 1720−1728

ascribed to the introduction of PDA layer, which can avoid the direct contact of Si NPs and electrolyte and alleviate the volume change of Si NPs, in favor of the formation of a stable SEI layer. The EIS results are quite consistent with the cyclic performances of the four samples, indicating that fast electron transfer and facile lithium ion diffusion path have been achieved for GO/PDA-Si_2, benefiting from the proper amount of GO and introduction of PDA coating layer.

CONCLUSION

In conclusion, we have successfully designed and synthesized GO/PDA-Si nanocomposite by an extremely facile and scalable solution-based method at room temperature. The as-prepared GO/PDA-Si_2 sample exhibits high specific capacity, good cyclic stability, and superior rate capability. A reversible discharge capacity of 1074 mAh g^{-1} was obtained after 300 cycles at a high current density of 2100 mA g^{-1}. The outstanding electrochemical performances can be attributed to the synergistic effect of the PDA and GO. The PDA layer provides a large number of secondary amine groups, which can form amide groups with carboxyl groups on GO and hydrogen bonds with hydroxyl groups on GO. The chemical bonding interactions firmly attach Si NPs on GO sheets so that particle aggregations during extended cycles can be prevented. The flexible polymer and GO layer can also provide a cushion effect to buffer the large volume change of Si NPs during the charge/discharge process. Furthermore, the PDA layer can facilitate the diffusion of lithium ions due to its good lithium ion conductivity. The strategy of simple surface modification by PDA is illustrated to be an effective way to realize the uniform distribution of Si NPs and create strong chemical interactions between Si and GO. This technique can be extended to the modification of other high-performance electrode materials.

AUTHOR INFORMATION

Corresponding Authors

*E-mail: chyfdeng@scut.edu.cn.

*E-mail: kechengh@ust.hk.

Notes

The authors declare no competing financial interest.

ACKNOWLEDGMENTS

This work was supported by the Guangzhou Scientific and Technological Planning Projects (Grants 2013J4100112 and 2014J4500002), the link project of Natural Science Foundation of China and Guangdong Province (Grant No. U1301244), and the Fok Ying Tung Foundation (Grant NRC07/08.EG01).

REFERENCES

(1) Tarascon, J. M.; Armand, M. Issues and Challenges Facing Rechargeable Lithium Batteries. *Nature* **2001**, *414*, 359−367.

(2) Tarascon, J. M.; Recham, N.; Armand, M.; Chotard, J. N. l.; Barpanda, P.; Walker, W.; Dupont, L. Hunting for Better Li-based Electrode Materials via Low Temperature Inorganic Synthesis. *Chem. Mater.* **2010**, *22*, 724−739.

(3) Baranchugov, V.; Markevich, E.; Pollak, E.; Salitra, G.; Aurbach, D. Amorphous Silicon Thin Films as a High Capacity Anodes for Li-ion Batteries in Ionic Liquid Electrolytes. *Electrochem. Commun.* **2007**, *9*, 796−800.

(4) Ma, H.; Cheng, F.; Chen, J. Y.; Zhao, J. Z.; Li, C. S.; Tao, Z. L.; Liang, J. Nest-like Silicon Nanospheres for High-capacity Lithium Storage. *Adv. Mater.* **2007**, *19*, 4067−4070.

(5) Peng, K.; Jie, J.; Zhang, W.; Lee, S. T. Silicon Nanowires for Rechargeable Lithium-ion Battery Anodes. *Appl. Phys. Lett.* **2008**, *93*, 033105.

(6) Cho, J. Porous Si Anode Materials for Lithium Rechargeable Batteries. *J. Mater. Chem.* **2010**, *20*, 4009−4014.

(7) Liu, N.; Wu, H.; McDowell, M. T.; Yao, Y.; Wang, C.; Cui, Y. A Yolk-shell Design for Stabilized and Scalable Li-ion Battery Alloy Anodes. *Nano Lett.* **2012**, *12*, 3315−3321.

(8) Chan, C. K.; Peng, H.; Liu, G.; McIlwrath, K.; Zhang, X. F.; Huggins, R. A.; Cui, Y. High-performance Lithium Battery Anodes Using Silicon Nanowires. *Nat. Nanotechnol.* **2008**, *3*, 31−35.

(9) Cui, L.; Ruffo, R.; Chan, C. K.; Hailin, P.; Cui, Y. Crystalline-Amorphous Core-Shell Silicon Nanowires for High Capacity and High Current Battery Electrodes. *Nano Lett.* **2009**, *9*, 491−495.

(10) Park, M. H.; Kim, M. G.; Joo, J.; Kim, K.; Kim, J.; Ahn, S.; Cui, Y.; Cho, J. Silicon Nanotube Battery Anodes. *Nano Lett.* **2009**, *9*, 3844−3847.

(11) Yao, Y.; McDowell, M. T.; Ryu, I.; Wu, H.; Liu, N.; Hu, L.; Nix, W. D.; Cui, Y. Interconnected Silicon Hollow Nanospheres for Lithium-ion Battery Anodes with Long Cycle Life. *Nano Lett.* **2011**, *11*, 2949−2954.

(12) Bruce, P. G.; Scrosati, B.; Tarascon, J. M. Nanomaterials for Rechargeable Lithium Batteries. *Angew. Chem., Int. Ed.* **2008**, *47*, 2930−2946.

(13) Kim, M. G.; Cho, J. Reversible and High-capacity Nanostructured Electrode Materials for Li-ion Batteries. *Adv. Funct. Mater.* **2009**, *19*, 1497−1514.

(14) Hu, Y. S.; Demir-Cakan, R.; Titirici, M. M.; Muller, J. O.; Schlogl, R.; Antonietti, M.; Maier, J. Superior Storage Performance of a Si@SiO_x/C Nanocomposite as Anode Material for Lithium-ion Batteries. *Angew. Chem., Int. Ed.* **2008**, *47*, 1645−1649.

(15) Magasinski, A.; Dixon, P.; Hertzberg, B.; Kvit, A.; Ayala, J.; Yushin, G. High-performance Lithium-ion Anodes Using a Hierarchical Bottom-up Approach. *Nat. Mater.* **2010**, *9*, 353−358.

(16) Stankovich, S.; Dikin, D. A.; Dommett, G. H.; Kohlhaas, K. M.; Zimney, E. J.; Stach, E. A.; Piner, R. D.; Nguyen, S. T.; Ruoff, R. S. Graphene-based Composite Materials. *Nature* **2006**, *442*, 282−286.

(17) Yoo, E. J.; Kim, J.; Hosono, E.; Zhou, H.; Kudo, T.; Honma, I. Large Reversible Li Storage of Graphene Nanosheet Families for Use in Rechargeable Lithium Ion Batteries. *Nano Lett.* **2008**, *8*, 2277−2282.

(18) Sun, Y.; Wu, Q.; Shi, G. Graphene Based New Energy Materials. *Energy Environ. Sci.* **2011**, *4*, 1113.

(19) Wang, J. Z.; Zhong, C.; Chou, S. L.; Liu, H. K. Flexible Free-standing Graphene-silicon Composite Film for Lithium-ion Batteries. *Electrochem. Commun.* **2010**, *12*, 1467−1470.

(20) Zhou, X.; Yin, Y. X.; Wan, L. J.; Guo, Y. G. Facile Synthesis of Silicon Nanoparticles Inserted into Graphene Sheets as Improved Anode Materials for Lithium-ion Batteries. *Chem. Commun.* **2012**, *48*, 2198−2200.

(21) Hu, R.; Sun, W.; Chen, Y.; Zeng, M.; Zhu, M. Silicon/Graphene Based Nanocomposite Anode: Large-scale Production and Stable High Capacity for Lithium Ion Batteries. *J. Mater. Chem. A* **2014**, *2*, 9118−9125.

(22) Tao, H. C.; Fan, L. Z.; Mei, Y.; Qu, X. Self-supporting Si/Reduced Graphene Oxide Nanocomposite Films as Anode for Lithium Ion Batteries. *Electrochem. Commun.* **2011**, *13*, 1332−1335.

(23) Zhou, M.; Pu, F.; Wang, Z.; Cai, T.; Chen, H.; Zhang, H.; Guan, S. Facile Synthesis of Novel Si Nanoparticles-Graphene Composites as High-Performance Anode Materials for Li-ion Batteries. *Phys. Chem. Chem. Phys.* **2013**, *15*, 11394−11401.

(24) Ye, Y. S.; Xie, X. L.; Rick, J.; Chang, F. C.; Hwang, B. J. Improved Anode Materials for Lithium-ion Batteries Comprise non-Covalently Bonded Graphene and Silicon Nanoparticles. *J. Power Sources* **2014**, *247*, 991−998.

(25) Zhu, Y.; Liu, W.; Zhang, X.; He, J.; Chen, J.; Wang, Y.; Cao, T. Directing Silicon-Graphene Self-assembly as a Core/Shell Anode for High-performance Lithium-ion Batteries. *Langmuir* **2013**, *29*, 744−749.

DOI: 10.1021/jp511179s
J. Phys. Chem. C 2015, 119, 1720−1728

(26) Zhao, G.; Zhang, L.; Meng, Y.; Zhang, N.; Sun, K. Decoration of Graphene with Silicon Nanoparticles by Covalent Immobilization for Use as Anodes in High Stability Lithium Ion Batteries. *J. Power Sources* **2013**, *240*, 212−218.
(27) Yang, S.; Li, G.; Zhu, Q.; Pan, Q. Covalent Binding of Si Nanoparticles to Graphene Sheets and Its Influence on Lithium Storage Properties of Si Negative Electrode. *J. Mater. Chem.* **2012**, *22*, 3420−3425.
(28) Wen, Y.; Zhu, Y.; Langrock, A.; Manivannan, A.; Ehrman, S. H.; Wang, C. Graphene-Bonded and -Encapsulated Si Nanoparticles for Lithium Ion Battery Anodes. *Small* **2013**, *9*, 2810−2816.
(29) Sun, C.; Deng, Y. F.; Wan, L. N.; Qin, X. S.; Chen, G. H. Graphene Oxide-immobilized NH_2-terminated Silicon Nanoparticles by Cross-linked Interactions for Highly Stable Silicon Negative Electrodes. *ACS Appl. Mater. Interfaces* **2014**, *6*, 11277−11285.
(30) Li, Z. F.; Zhang, H.; Liu, Q.; Liu, Y.; Stanciu, L.; Xie, J. Novel Pyrolyzed Polyaniline-grafted Silicon Nanoparticles Encapsulated in Graphene Sheets as Li-ion Battery Anodes. *ACS Appl. Mater. Interfaces* **2014**, *6*, 5996−6002.
(31) Liu, Y.; Ai, K.; Lu, L. Polydopamine and Its Derivative Materials: Synthesis and Promising Applications in Energy, Environmental, and Biomedical Fields. *Chem. Rev.* **2014**, *114*, 5057−5115.
(32) Lei, C.; Han, F.; Li, D.; Li, W. C.; Sun, Q.; Zhang, X. Q.; Lu, A. H. Dopamine as the Coating Agent and Carbon Precursor for the Fabrication of N-doped Carbon Coated Fe_3O_4 Composites as Superior Lithium Ion Anodes. *Nanoscale* **2013**, *5*, 1168−1175.
(33) Kong, J.; Yee, W. A.; Yang, L.; Wei, Y.; Phua, S. L.; Ong, H. G.; Ang, J. M.; Li, X.; Lu, X. Highly Electrically Conductive Layered Carbon Derived from Polydopamine and Its Functions in SnO_2-based Lithium Ion Battery Anodes. *Chem. Commun.* **2012**, *48*, 10316−10318.
(34) Hummers, W. S.; Offeman, R. E. Preparation of Graphitic Oxide. *J. Am. Chem. Soc.* **1958**, *80*, 1339.
(35) Chuang, I. S.; Maciel, G. E. Probing Hydrogen Bonding and the Local Environment of Silanols on Silica Surfaces via Nuclear Spin Cross Polarization Dynamics. *J. Am. Chem. Soc.* **1996**, *118*, 401−406.
(36) Xu, W.; Riikonen, J.; Nissinen, T.; Suvanto, M.; Rilla, K.; Li, B.; Wang, Q.; Deng, F.; Lehto, V. P. Amine Surface Modifications and Fluorescent Labeling of Thermally Stabilized Mesoporous Silicon Nanoparticles. *J. Phys. Chem. C* **2012**, *116*, 22307−22314.
(37) Wang, Q.; Plylahan, N.; Shelke, M. V.; Devarapalli, R. R.; Li, M.; Subramanian, P.; Djenizian, T.; Boukherroub, R.; Szunerits, S. Nanodiamond Particles/Reduced Graphene Oxide Composites as Efficient Supercapacitor Electrodes. *Carbon* **2014**, *68*, 175−184.
(38) Ren, H.; Kulkarni, D. D.; Kodiyath, R.; Xu, W.; Choi, I.; Tsukruk, V. V. Competitive Adsorption of Dopamine and Rhodamine 6G on the Surface of Graphene Oxide. *ACS Appl. Mater. Interfaces* **2014**, *6*, 2459−2470.
(39) Wang, L.; Wang, D.; Dong, Z.; Zhang, F.; Jin, J. Interface Chemistry Engineering for Stable Cycling of Reduced GO/SnO_2 Nanocomposites for Lithium Ion Battery. *Nano Lett.* **2013**, *13*, 1711−1716.
(40) Chou, S. L.; Wang, J. Z.; Choucair, M.; Liu, H. K.; Stride, J. A.; Dou, S. X. Enhanced Reversible Lithium Storage in a Nanosize Silicon/Graphene Composite. *Electrochem. Commun.* **2010**, *12*, 303−306.

DOI: 10.1021/jp511179s
J. Phys. Chem. C 2015, 119, 1720−1728